Quarterly Report for

July 1997 - September 1997

Stanford Geothermal Program

DE-FG07-95ID13370

TABLE OF CONTENTS

1. EXPERIMENTAL STUDY OF BOILING IN POROUS MEDIA

This research project is being conducted by Dr. Cengiz Satik. The objective of this study is to improve our understanding of the process of boiling in porous media by using both experimental and numerical methods.

1.1 SUMMARY

The ultimate goal of this work is to understand the origin of the two important but currently unknown functions of relative permeability and capillary pressure. During the current quarter, three experiments using a Berea sandstone core sample were conducted upon the completion of further improvements and modifications to the apparatus. The results of these experiments will be discussed here.

1.2 INTRODUCTION

The process of boiling in porous media is of significance in geothermal systems as well as in many other applications such as porous heat pipes, drying and nuclear waste disposal. Despite its importance in these applications, the fundamentals of this process are poorly understood. Most of the problems arise from the lack of the understanding of the mechanics and dynamics of this complex process.

A look at the previous literature shows that many attempts have been made in both experimental and theoretical directions to investigate and to describe the process of boiling in porous media (Satik, 1994). Most previous studies have used continuum formulations which made use of Darcy's law extended to multiphase flow with relative permeability and capillary pressure functions derived from isothermal gas-liquid displacement processes. These processes have major differences to boiling displacement which involves additional phenomena such as heat transfer, nucleation and phase change. Moreover, the continuum approaches are also limited by the assumption of capillary control at the pore level (low Capillary and Bond numbers). Due to these restrictions and uncertainties, it is unclear whether the relative permeability and capillary pressure functions currently used for modeling the process of boiling in porous media are appropriate. At the same time, fundamental studies focusing at the microscopic pore scale have been very limited. In a recent study by Satik and Yortsos (1996), numerical and experimental pore networks were used to model boiling in porous media at a microscopic scale. Satik and Yortsos (1996) developed a numerical pore network model for boiling in a horizontal, two-dimensional porous medium and conducted visualization experiments by using glass micromodels. Although progress was made, their model was developed only for a single bubble growth problem in a horizontal porous medium, ignoring the effects of gravity. Therefore, further work is still needed to improve the understanding and to resolve the issues raised by the continuum formulations (see Satik, 1994, for details) and eventually to obtain appropriate forms of the relative permeability and capillary pressure functions.

In this work, we conducted boiling experiments with real core samples from a Berea sandstone. Using an X-ray computer tomography (CT) scanner, we visualized the process

and determined the three-dimensional fluid distributions within the core while the experiment was in progress. By using thermocouples, pressure transducers and heat flux sensors under the control of a data-acquisition system, we obtained temperature, pressure and heat flux values along the core. The comparison of the experimental data with the results of numerical simulation will give us an opportunity to check the numerical results and infer the relative permeability and capillary pressure functions.

1.3 RESULTS

Three experiments were conducted during the last quarter. The core was positioned horizontally during the first experiment while it was positioned vertically during the last two experiments. During the first vertical experiment, the heater element was placed at the top of the core holder. After the completion of this experiment, the core was rotated 180 degrees so that the heater would be positioned at the bottom. As reported in the last quarterly report, unusual negative pressures were measured during the bottom-heating vertical experiment conducted in June 1997. Therefore, the last vertical (bottom-heating) experiment in the last quarter was repeated in a bottom-heating case to check the consistency of the results with those from the experiment conducted in June 1997. All of these experiments consisted of both heating (increasing heat flux) and cooling (decreasing heat flux) stages. Both heating and cooling stages consisted of several step-like increases in heater power. Following the completion of a cooling stage in each experiment the core was dried at high temperature (~110^{o}C) and under vacuum conditions. The core was checked for leaks both under high pressure and vacuum conditions before it was used in an experiment. The results obtained from these three experiments are discussed in this section.

A schematic of the experimental apparatus and procedure were given in the previous quarterly report. Briefly, the apparatus consists of a core holder, a data acquisition system, a vacuum pump, a liquid pump and a balance. Eleven pressure taps are placed along the core length to measure pressures and temperatures, respectively. A heater and a heat flux sensor are placed in the specially designed inlet end of the core holder. In addition, eleven heat flux sensors with built-in thermocouples are placed along the core to measure heat losses and temperatures. In order to obtain more information close to the heater end, the first eight pressure taps, thermocouples and heat flux sensors are placed every 3 cm from the heater while the remaining three are 6 cm apart from each other. During an experiment, the core holder is placed inside the high resolution X-ray CT equipment to obtain *in-situ* saturation profiles along the core (Satik, 1997). Two pictures of the apparatus mounted on to the scanner are shown in Figure 1.1.

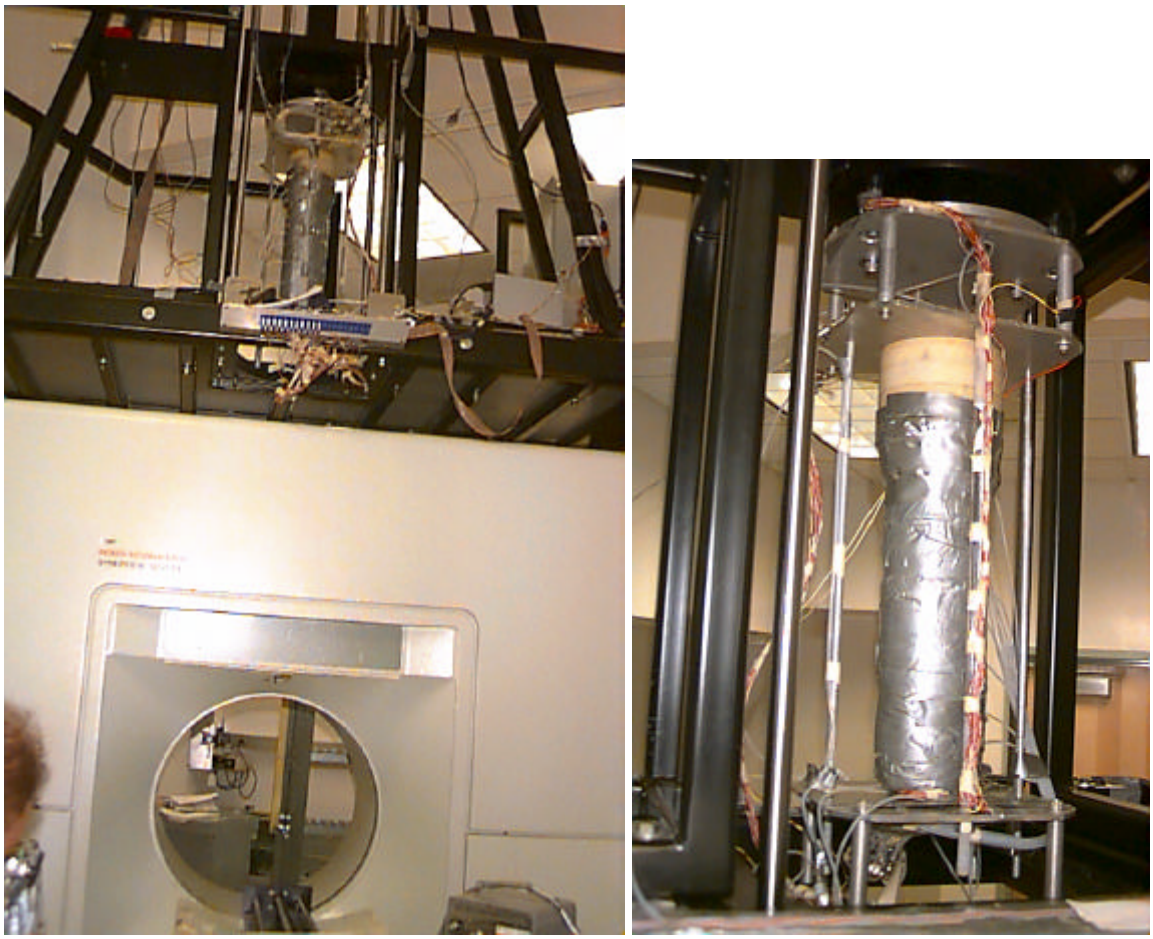

Figure 1.1: Pictures of the experimental apparatus mounted in the X-ray CT scanner.

The core used in these experiments was a Berea sandstone core with a permeability of about 780 md. Before the first experiment, the core was preheated at 450^{o}C overnight to deactivate clays. After assembling the core holder and auxiliary equipment, the core was mounted into the X-ray CT scanner and was kept under vacuum conditions for several hours to remove the air inside the pore space. After being scanned to obtain dry CT values, the core was saturated completely with deaerated water. The core was then scanned again to obtain wet CT values. Using these two sets of CT values, the porosity distribution of the core was obtained by using the method described in Satik (1997). This procedure was followed during each of the experiments. Figure 1.2 shows three-dimensional porosity images of the core obtained before each of the three experiments. The images look very similar, indicating that drying process conducted between each experiment was successful. This is also apparent from the average porosity profiles given in Figure 1.3. These profiles were obtained by taking a simple average of the porosity distribution at each circular slice along the core. The porosity profile obtained from the horizontal experiment deviates by a maximum of about 3% from the other two profiles. This difference may be attributed to the errors introduced by the horizontal positioning system of the CT scanner as well as to the core not being 100% saturated with water. The average porosity of the core was found to be around 22%.

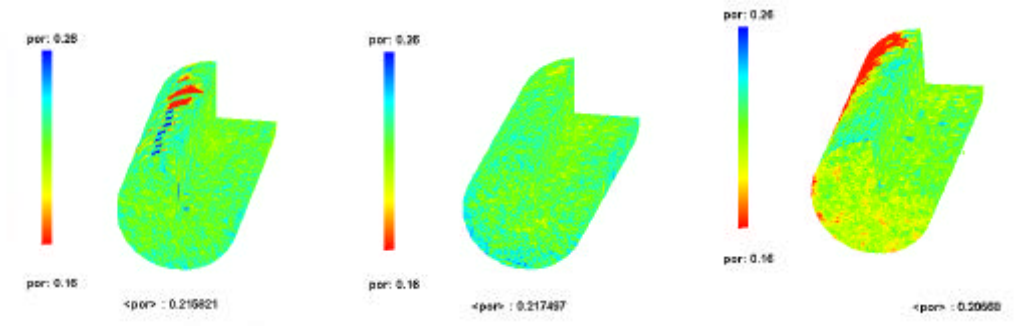

(a) *(b)* *(c)*

Figure 1.2: Three-dimensional porosity distributions of the core used, obtained before (a) bottom-heating vertical, (b) top-heating vertical and (c) side-heating horizontal boiling experiments.

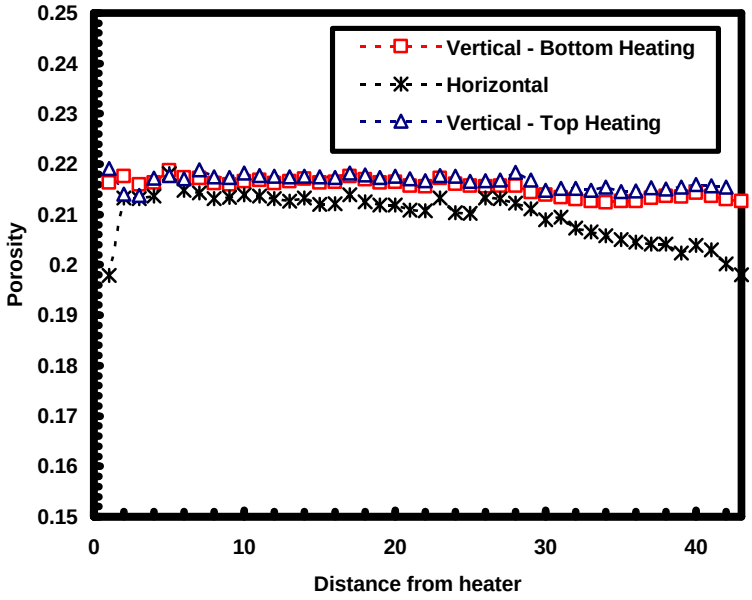

Figure 1.3: Average porosity profiles obtained during the initial warm-up stage of the experiment.

Figure 1.4 shows time histories of heater power setting, heat flux at the heater, wall temperature, pressure and liquid mass produced during the bottom-heating vertical, top-heating vertical and side-heating horizontal boiling experiments, respectively. During the initial warming-up stage, power to the heater was increased slowly to avoid thermal shock to the epoxy core holder. The core was CT scanned several times to check any possible gas (air) formation inside the pore space at temperatures lower than the actual boiling temperature. The three-dimensional saturation profiles obtained during the initial warming-up stages of all of the experiments did not show a presence of gas phase inside the pore space. This result confirmed that the air both inside the pore space and in the

water used to saturate it had been successfully removed. As shown in Figure 1.4, during all of the experiments the heater power was changed incrementally from 0% to 60%, waiting at least 24 hours at each heater power setting. The total output of the heater at 100% setting was measured to be 30 watts. These long waiting times allowed the system sufficient time to reach steady state conditions. During the process of increasing heater power, the core was scanned to obtain CT values and three-dimensional steam saturations were calculated by using the method described in Satik (1997). At each power setting, steady state conditions were confirmed by examining the temperature, pressure, liquid mass-produced from the core and heat flux readings (flattening portions of the curves in Figure 1.4). Temperature and heat flux profiles in Figure 1.4 show consistent results, a sharp increase as heater power changes and a flattening after some time to reach steady state. Pressures and liquid mass-produced curves indicate clearly the formation of first steam phase as an increase in the values followed by a flattening to stabilize to a steady state. The sudden drop in both pressures and liquid mass-produced values for the bottom-heating vertical experiment (at around 50 hours) was due to a leak formed along the eleventh pressure line (Pw11). This pressure port was located at the furthest distance from the heater. To continue the experiment, the eleventh pressure port was sealed off since it would not affect the experimental results.

At the end of each power setting X-ray scans were taken at 42 locations and three-dimensional steam saturation images were constructed using the method described in Satik (1997). Figure 1.5 shows a comparison of the steam saturation distributions at the same heater power settings of 45, 50, 55 and 60% (from top to bottom) during the three experiments. These images show some interesting features. The two-phase zone length was the largest during the horizontal boiling experiment. The interface between the two-phase zone and liquid zone was sharp for both side-heating horizontal and top-heating vertical experiments while some steam override effects, due to the buoyancy forces, were observed during the bottom-heating vertical experiment.

A comparison of the average steam saturation, pressure and temperature profiles along the core obtained from the three experiments is shown in Figure 1.6. The expected results were obtained. A two-phase zone followed by single-phase liquid zone was obtained at lower heat fluxes while a two-phase zone between single-phase steam and liquid zones was obtained at higher heat fluxes. These results are also apparent from the temperature profiles shown in Figure 1.6. The profiles at early times have the characteristic of a two phase region (almost flat temperature profile) followed by a single-phase liquid zone while profiles at later times indicate a two-phase region (almost flat profile) between single-phase steam and water regions. Once a dry steam zone forms the temperature gradient over this zone becomes large due to the relatively small thermal conductivity of steam. Pressure profiles are also consistent.

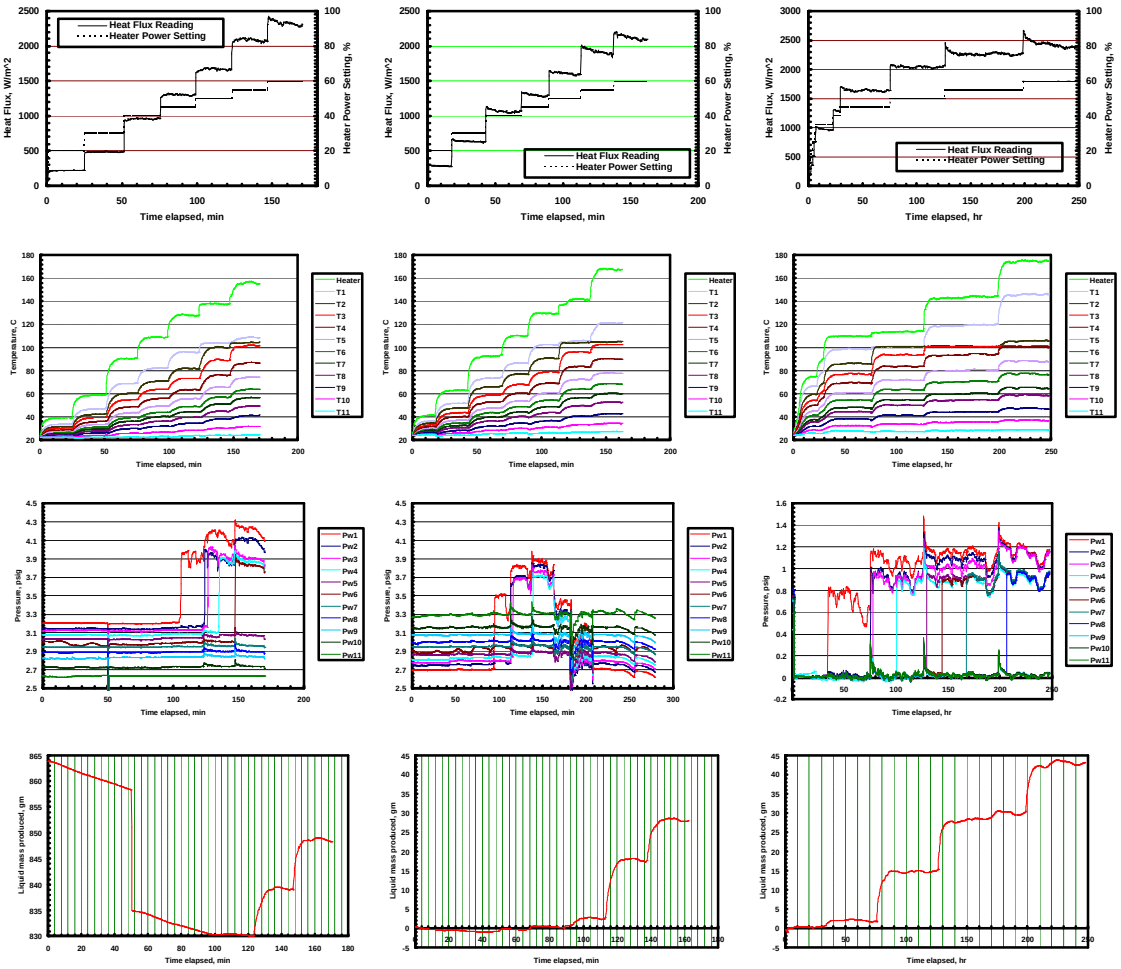

(a) *(b)* *(c)*

Figure 1.4: Histories of heater power setting, heat flux at the heater, wall temperature, pressure and liquid mass produced during (a) bottom-heating vertical, (b) top-heating vertical and (c) side-heating horizontal boiling experiments.

1.4 FUTURE WORK

During the next quarter, we will continue to analyze the results presented in this report. We will make use of the TOUGH2 numerical simulator to understand the results better. Also, to study boiling in fractured porous media, the core used in the experiments reported here will be cut into two halves and the two pieces will be bonded together again to create an artificial fracture (or gap). Another boiling experiment will be conducted. Finally, the numerical simulator will be used to match the experimental data, as described later in Section 3 of this report.

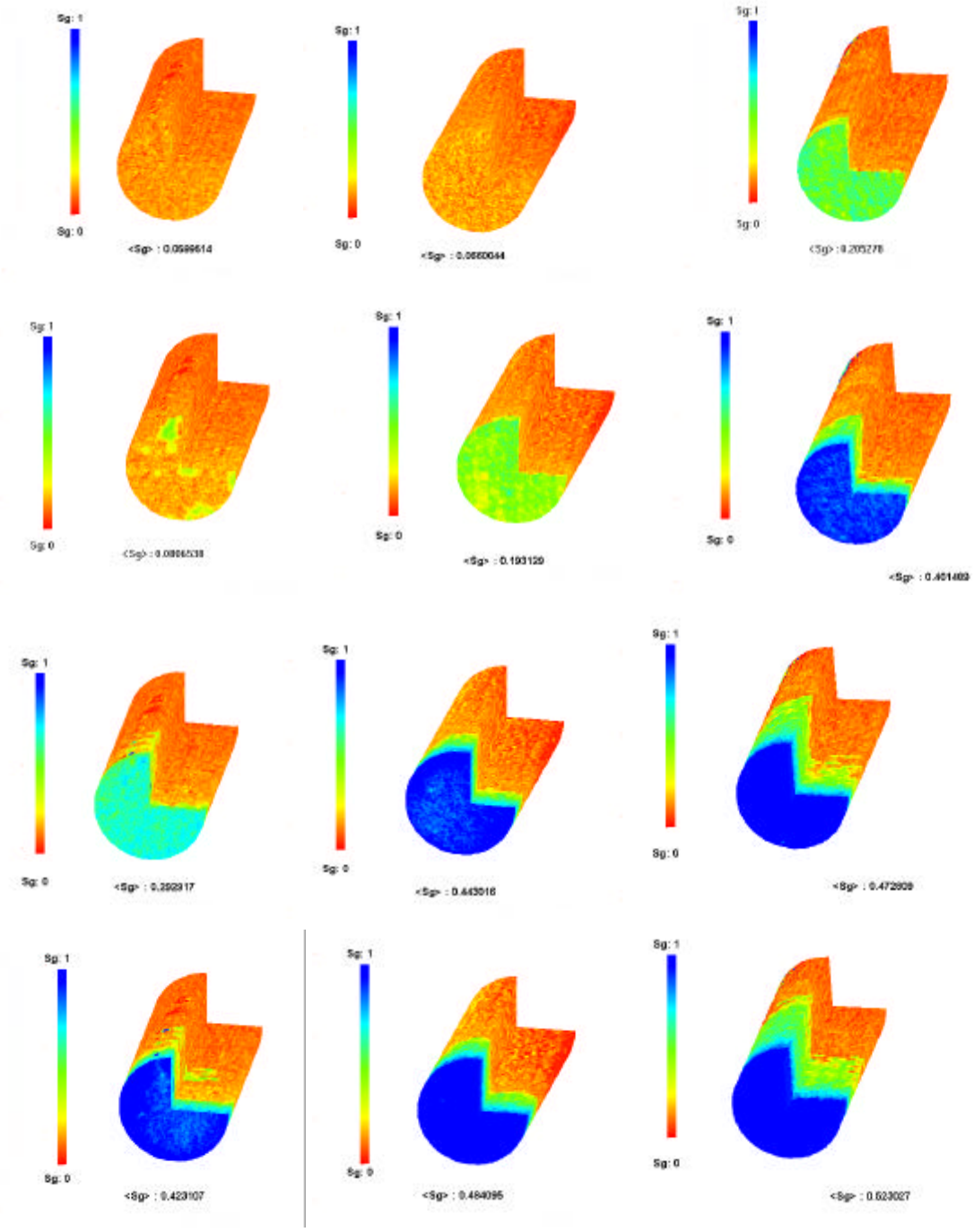

(a) *(b)* *(c)*

Figure 1.5: Three-dimensional steam saturations obtained at four different heater power settings during (a) bottom-heating vertical, (b) top-heating vertical and (c) side-heating horizontal boiling experiments.

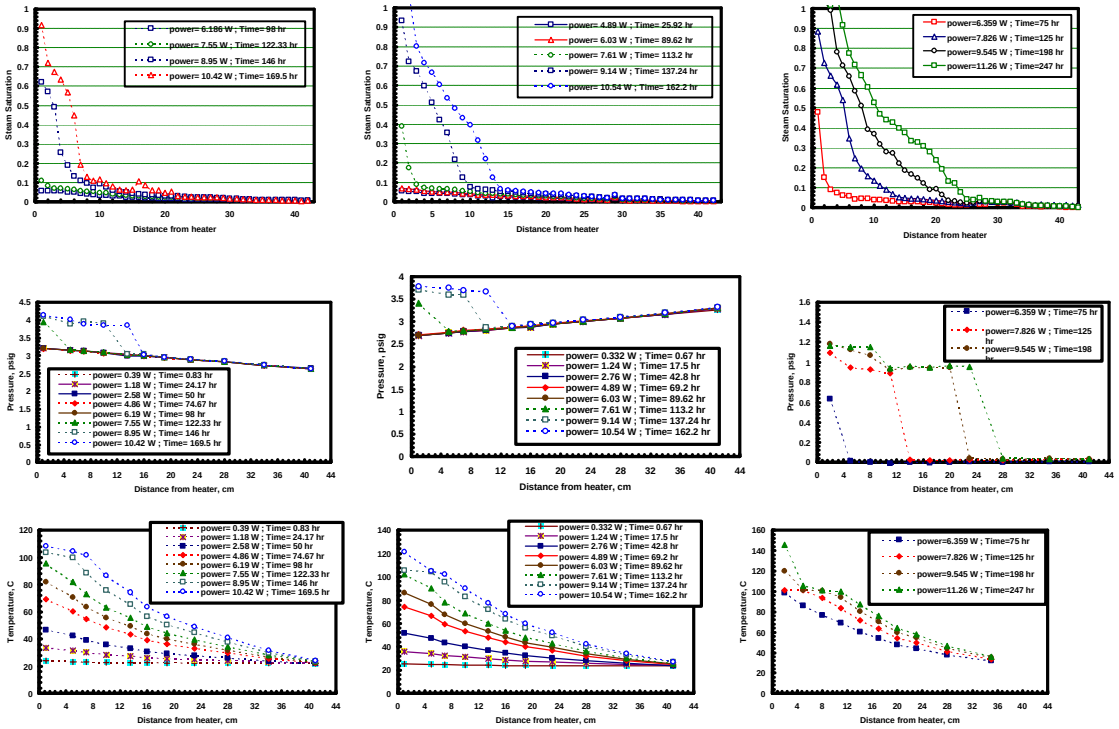

(a) *(b)* *(c)*

Figure 1.6: Steam saturation, pressure and temperature profiles obtained during (a) bottom-heating vertical, (b) top-heating vertical and (c) side-heating horizontal boiling experiments.

2. MEASUREMENTS OF STEAM-WATER RELATIVE PERMEABILITY

This research project is currently being conducted by Dr. Cengiz Satik and Professor Roland Horne. The aim of this project is to measure relative permeability relations for steam and water flowing simultaneously in a porous medium.

2.1 SUMMARY

A set of steady state experiments conducted under conditions that eliminate most errors associated with saturation and pressure measurements were attempted. However, difficulties were encountered as discussed in the last quarterly report. Problems with the previous attempts were identified in three main areas. First, it is crucial that the core used in the experiments behave normally during fluid injection (free of complications with clays, heterogeneities etc.). Second, the core holder needs to withstand high temperatures and pressures for long times (on the order of two weeks). Lastly, the experimental method needs to be accurate enough to make the relative permeability calculations. The first problem was solved by X-ray scanning the core to determine whether it was homogenous when received and then assembling the core holder with homogenous core samples only. Clay complications (swelling, particle migration) were solved by preheating the core samples at 800 ^{o}C (instead of 450 ^{o}C). To resolve the second problem a new core holder design was implemented during the last quarter. In the first attempt, a core sample was placed in a high temperature plastic (ultem) tubing and the annulus between the core and the tube was filled with high temperature epoxy (Cotronix 4400). Following the completion of this core holder, a preliminary experiment was conducted. The experiment failed after two days due to leaks induced by a crack formed at one of the pressure ports. To examine the core holder visually, it was cut into two pieces after the experiment. The epoxy in some of the pressure ports, especially those closer to the injection end where temperatures were higher and in the injection port itself, was found to have lost its integrity, which was later found to be the cause of the core holder failure. Therefore, another type of epoxy (Cotronix 4461) was tested in the next core holder. The new core holder was manufactured and checked at high temperatures and pressures for extended times and the new design has proven to be satisfactory. Improvements to the injection and production end plates were also made. To solve the last problem of methodology we needed first to resolve the core design issues and needed to have a core and core holder that are flexible enough for extreme experimental conditions. Upon the completion of such a system, two types of injection end plates were manufactured, one set with one injection port and one set with two injection ports. These new plates will be used in the methods described in the previous quarterly report. During the last quarter, we have tested the end plate with two injection ports only. This end plate has two specially designed D-shaped sections separated by two O-rings. We have conducted several preliminary experiments with the new system. The results of the latest experiment are presented in Section 2.2.

As discussed in the last quarterly report, the previous experimental apparatus consisted of an injection unit with one furnace to generate a mixture of steam and hot water at a known fraction. The steam fraction or the power to the furnace was controlled by a voltage

controller with an ammeter. In the new design, dry steam and hot water were generated separately using two furnaces. The steam and hot water were then injected into the core through the two different ports of the inlet end plate. These two ports are separated by two D-shaped O-rings, making sure that mixing of the two fluids takes place inside the porous medium rather than in the inlet port itself.

During an experiment, heat losses along the core body will be measured by using eight heat flux sensors. Temperatures and pressures will be measured by thirteen T-type thermocouples and Celesco transducers. Four of these will be placed in the injection lines, eight over the core body (inserted through the pressure lines), and one at the outlet of the core. Nine heat flux sensors with built-in thermocouples will be placed at equal intervals along the plastic core holder to measure heat losses and temperatures. Proportional voltage signals from the heat flux sensors, thermocouples and pressure transducers will be conditioned and collected by a data acquisition system. The data will then analyzed in a personal computer using "LabView", a graphical programming software.

The core (Berea sandstone) samples used in the preliminary experiments were 43.18 cm in length and 5.08 cm in diameter. During the preparation of a core holder, core samples were first heated to 800^{o}C for twelve hours to deactivate clays and to get rid of residual water. Air initially dissolved in the injected water was not removed during the preliminary experiment, however it will be removed by boiling and cooling it before injecting into the core during an actual experiment to be conducted in the X-ray room, which is scheduled in mid-November 1997. Also, the core was dried under high temperature and vacuum conditions after the last preliminary experiment. A porosity measurement was conducted using the CT. Results will be presented below.

2.2 PRELIMINARY RESULTS

Several preliminary steam-water flow experiments were conducted to test the new experimental apparatus and method. Here we report on the results of the latest experiment only. This experiment was conducted using the final core holder and end plate designs, some details of which were discussed in the previous section. Steam and hot water were generated separately using two furnaces and were injected into the core from two isolated ports. The specially designed inlet end plate enabled us to mix the fluids inside the porous medium. During the experiment, we monitored two fluid pressure and temperatures before entering the core and two fluid pressure and temperatures along the core. T-type thermocouples were inserted through the pressure lines such that both measurements were taken at the same location. In the end, the experiment was terminated successfully without any leaks.

Figures 2.1 and 2.2 show the histories of steam and hot water furnace current and injection rates, respectively. During the experiment several combinations of flow rate and furnace power were tried to change the steam fraction injected. To decrease steam fraction, the water flow rate was kept constant while the steam flow rate was reduced incrementally down to 1 cc/min. At each change, sufficient waiting time was allowed for

the system to reach steady state conditions. Histories of the temperatures and pressures measured during the experiment are shown in Figures 2.3 and 2.5. All of the measurements showed slight oscillations except the water temperature. Water temperature seemed to be very unstable due to hot water boiling and condensing. To remedy this problem, power to the hot water furnace was reduced, decreasing the temperature, until a stable reading was obtained.

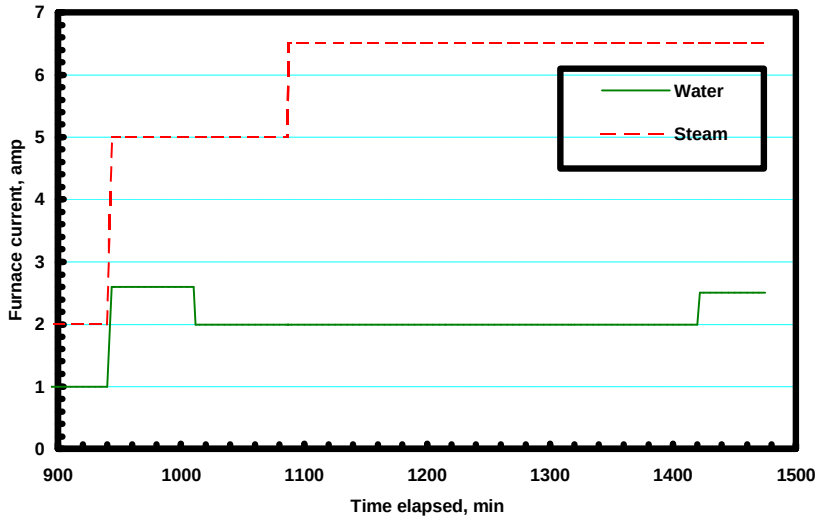

Figure 2.1: Histories of current passing through steam and hot water furnaces during the preliminary experiment .

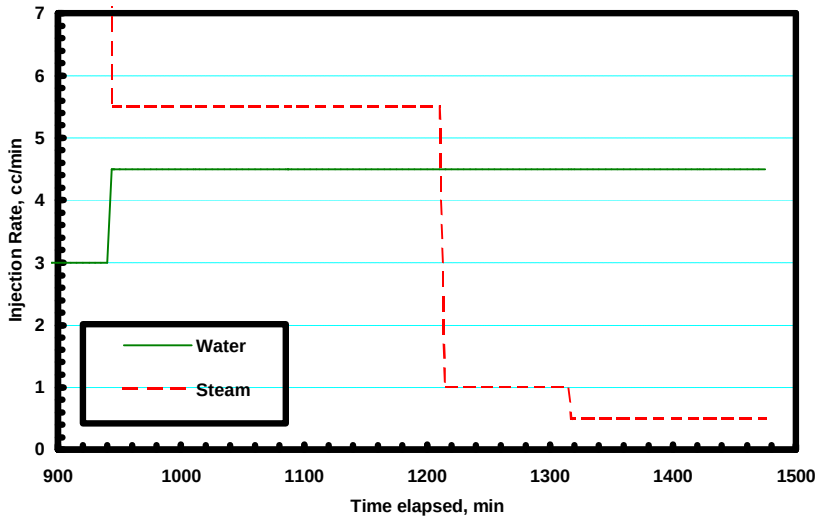

Figure 2.2: Histories of steam and hot water injection rates during the preliminary experiment.

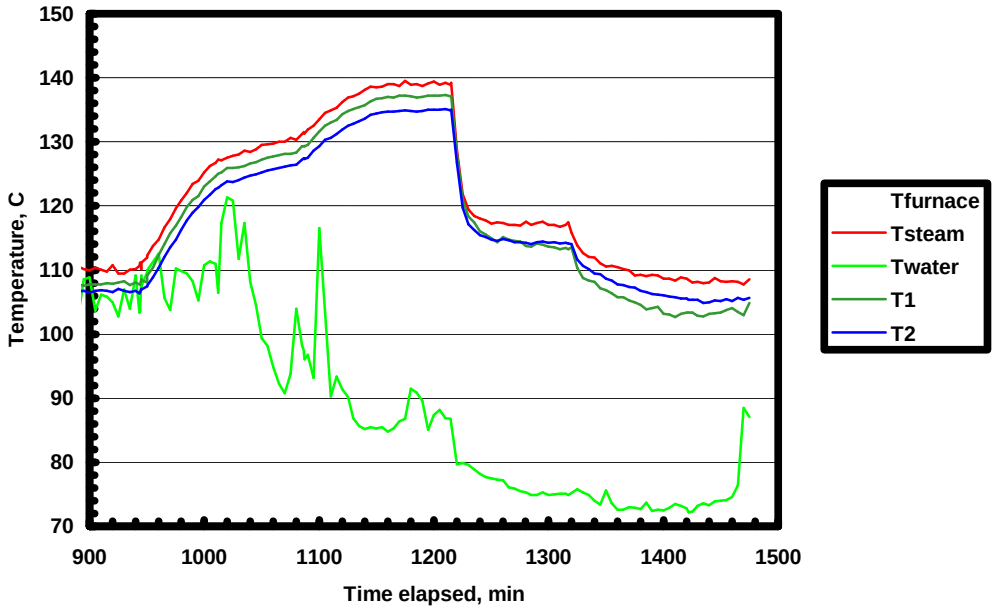

Figure 2.3: Histories of temperatures measured during the preliminary experiment. Tsteam, Twater, T1 and T2 represent steam and hot water temperatures at the core inlet face, the first two temperatures along the core body, respectively.

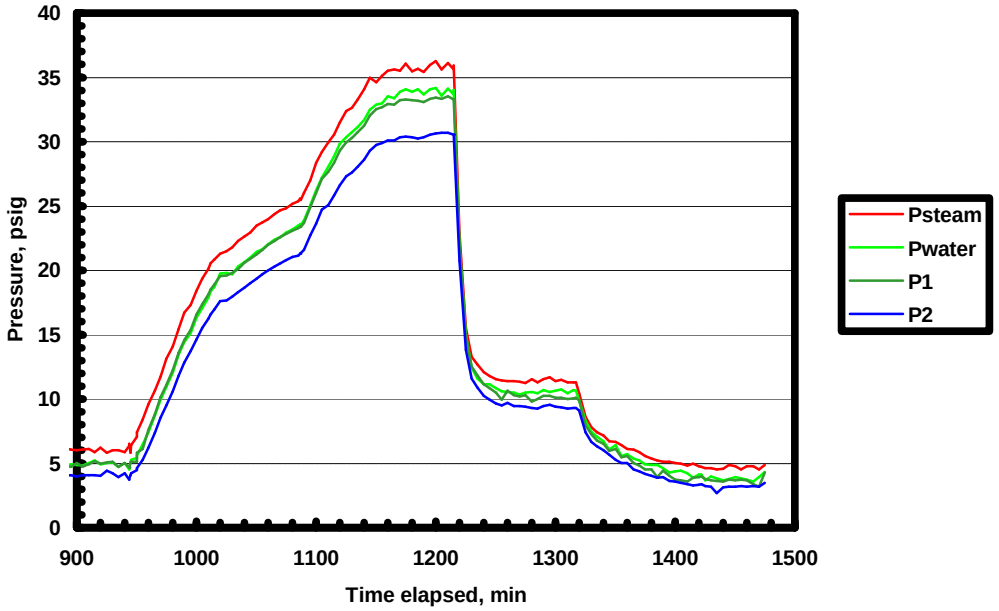

Figure 2.4: Histories of pressures measured during the preliminary experiment. Psteam, Pwater, P1 and P2 represent steam and hot water pressures at the core inlet face, the first two pressures along the core body, respectively.

Figures 2.5(a) and (b) show histories of the pressure measurements and the saturation pressures corresponding to temperature readings taken at the same locations. These plots

indicate the identity of the phase (vapor, liquid or two-phase) at each location. It seems that, during the experiment, the fluid in the steam injection line was always slightly superheated while the fluid in the hot water injection line was always subcooled water before entering the core, which indicated the success of the experimental method. On the other hand, Figure 2.5(b) shows that fluids in both pressure ports were slightly superheated steam until about 1200 min, at which time steam flow rate was reduced significantly (see also Figure 2.2). This caused a decrease in the steam fraction, which in turn changed the fluid phase conditions to be saturated two-phase mixture at port 1 and to be liquid water at port 2.

After the completion of the preliminary experiment, the core was dried in an oven at 110^{o}C and under vacuum conditions. Following the drying process the core holder was X-ray scanned dry and wet (100% saturated with deaerated water) to measure the porosity distributions and to check the integrity of the core holder. Figure 2.6 shows porosity images of the core at four locations along the core length. The area shown in the images intentionally includes the plastic tubing core holder to visualize all of the core holder. Although there seems to be a movement in the position of the core holder during the scanning, the images indicate a homogenous core. Therefore, we conclude that the core holder is still intact.

2.3 FUTURE WORK

During the next quarter, a full scale experiment, using the X-ray CT scanner, is scheduled in mid-November 1997. Modifications and improvements to the two furnaces used to generate steam and hot water are currently in progress. A new pressure measurement system using the new 10 psid pressure transducers will be finished and tested in the following weeks. We are also manufacturing another core holder.

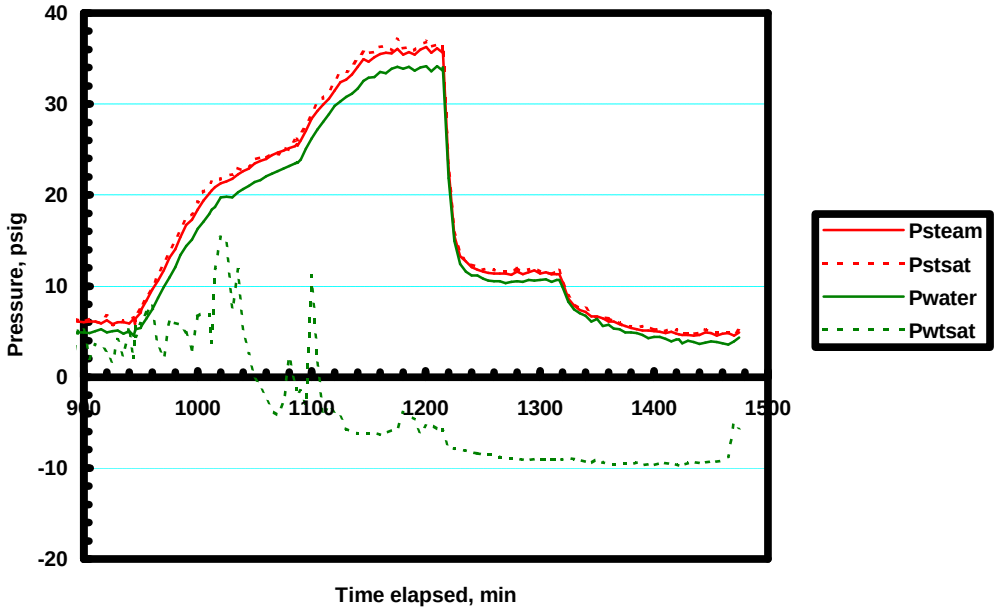

(a)

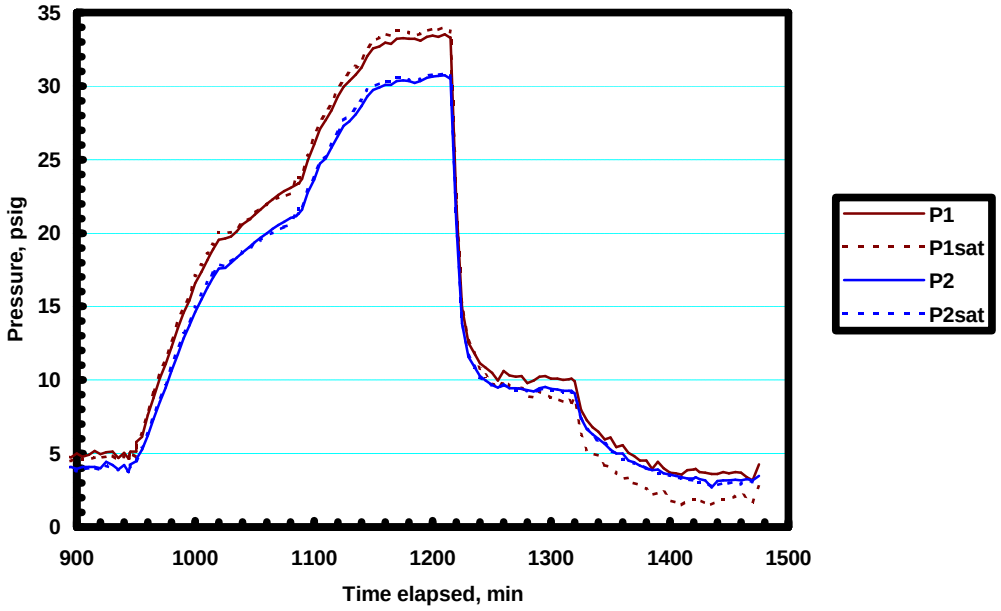

(b)

Figure 2.5: Histories of pressures and saturation pressures measured during the preliminary experiment (a) at the injection lines and (b) along the core body. Psteam, Pwater, P1 and P2 represent steam and hot water pressures at the core inlet face, the first two pressures along the core body, respectively. Subscript sat denotes to the saturation pressure values.

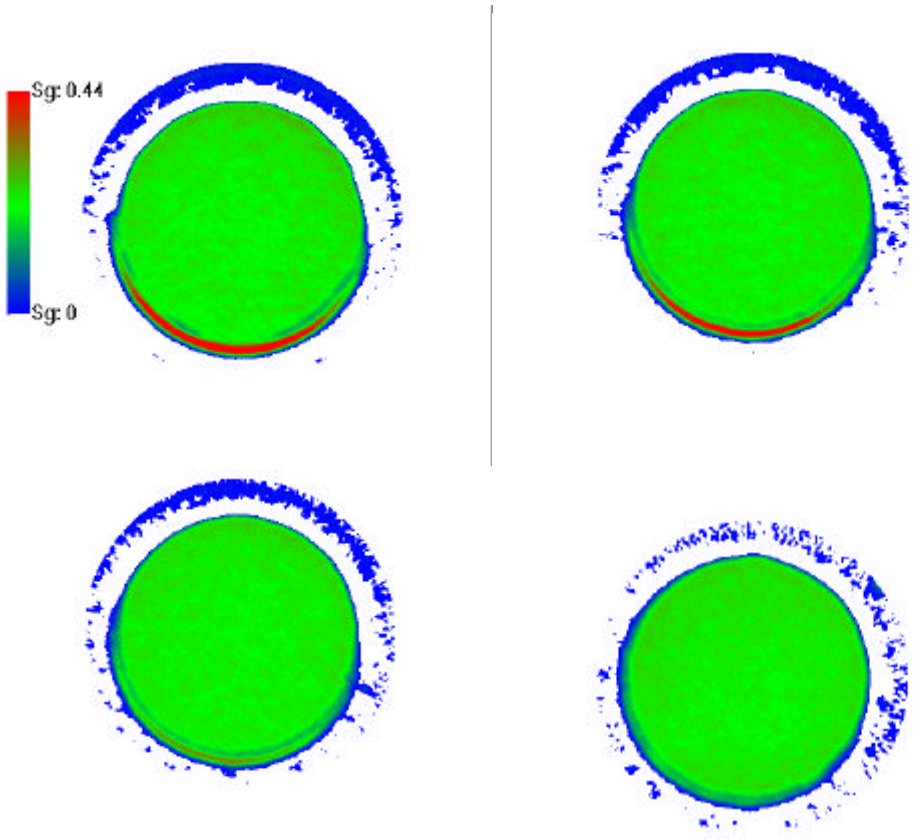

Figure 2.6: Porosity distributions obtained at four locations using X-ray CT scanner after the preliminary experiment.

3. INFERRING RELATIVE PERMEABILITIES FROM DYNAMIC EXPERIMENTS

This research project is being conducted by Research Assistant Marilou Guerrero, Dr. Cengiz Satik, and Prof. Roland Horne. The objective of this study is to simulate results obtained from the vertical boiling experiment using the commercial simulator, TOUGH2. This is done to give us a better understanding of boiling in porous media and to ultimately determine the appropriate relative permeability and capillary pressure functions for steam-water systems.

3.1 SUMMARY

An objective of this project is to simulate the boiling process in the vertical experiment conducted described in Section 1. In this study, numerical results using combinations of known relative permeability and capillary pressure functions were compared with the experimental results. Although many relative permeability and capillary pressure parameters and functions combinations were used in this study, only the final results are included here. Results show that using the Brooks-Corey relative permeability and capillary pressure functions gives the closest matches to the experimental observations of temperature and steam saturation.

3.2 EXPERIMENTAL SET-UP

In the actual experiment, a 49.5 cm long Berea sandstone core with radius 25.4 cm was sealed with epoxy and insulated with a ceramic fiber blanket. It was first saturated with liquid water and then heated at the bottom. Water was allowed to flow from the top end of the core, which was maintained at atmospheric conditions. The heater was insulated to reduce heat loss. During the 476.6 hour experiment, temperature, water pressure and steam saturation were measured at 43 points along the length of the core. The power level was increased 12 times from 0.3465 J/sec to 0.1126 J/sec.

3.3 TOUGH2 MODEL

The TOUGH2 simulation grid used is a two-dimensional radial model with 4 rings and 51 layers. The first (innermost) ring represents the core; the second ring represents the epoxy; the third ring represents the insulator; and the fourth ring represents the surrounding air. The first 50 layers are core layers while the 51st layer is the air layer. To simulate a constant pressure boundary the 51st layer was assigned a much larger volume than the core layers. Since there is no fluid flow along the radial directions, permeability values were assigned only along the angular and vertical directions.

3.4 RESULTS AND DISCUSSION

The Brooks-Corey relative permeability functions are given as:

$$k_{rl} = S_{ek}^{(2-3\,l)/\,l} \tag{3.1}$$

$$k_{rg} = \begin{cases} (1-S_{ek})^2(1-S_{ek}^{(2-3\lambda)/\lambda}) & \text{if } RP(3)=0 \\ 1-k_{rl} & \text{if } RP(3)\neq 0 \end{cases} \quad (3.2)$$

The Brooks-Corey capillary pressure functions are given as

$$p_c = \begin{cases} -p_e[e/(1-S_{lrc})]^{-1/\lambda} - (p_e/\lambda)[e/(1-S_{lrc})]^{(1-\lambda)/\lambda}(S_l - S_{lrc} - e) & \text{for } S_l < (S_{lrc}+e) \\ -p_e(S_{ek})^{(2-3\lambda)/\lambda} & \text{for } S_l \geq (S_{lrc}+e) \end{cases} \quad (3.3)$$

where

$$S_{ec} = (S_l - S_{lrc})/(1-S_{lrc}) \quad (3.4)$$

$$S_{ek} = (S_l - S_{lrk})/(1-S_{lrk}-S_{gr}) \quad (3.5)$$

and S_l is the liquid saturation; S_{lrk} is the residual liquid saturation in the relative permeability function; S_{gr} is the residual gas saturation; S_{lrc} is the residual liquid saturation in the capillary pressure function; λ is the pore size distribution index; and p_e is the gas entry pressure. The TOUGH2 default for ε is 0.01.

Figures 3.1 and 3.2 show the relative permeability and capillary pressure curves, respectively, used in this study. The parameters are as follows: S_{lrk}=0, S_{gr}=0, RP(3)=0, λ=0.55, and p_e=250 Pa.

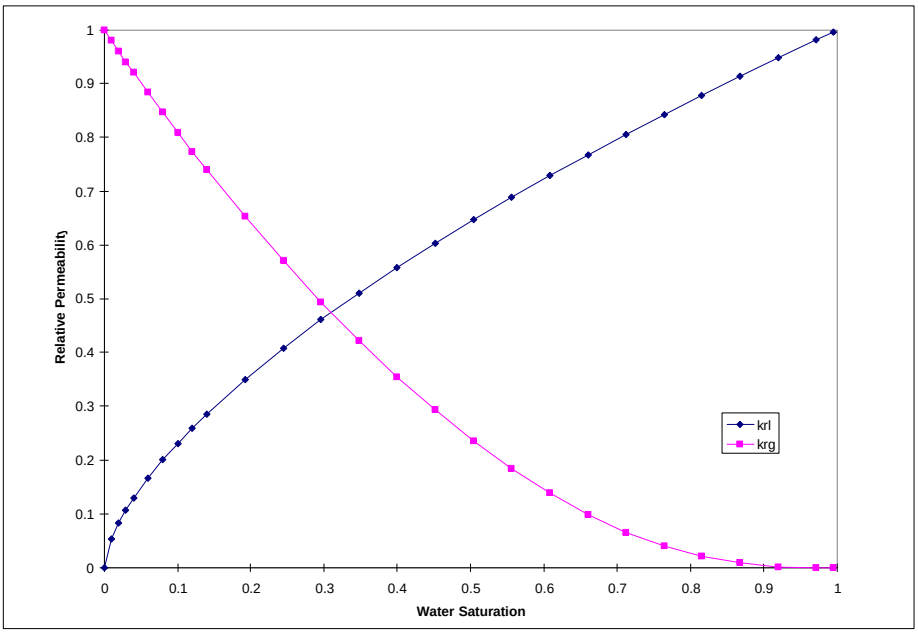

Figure 3.1: Brooks-Corey relative permeability curve.

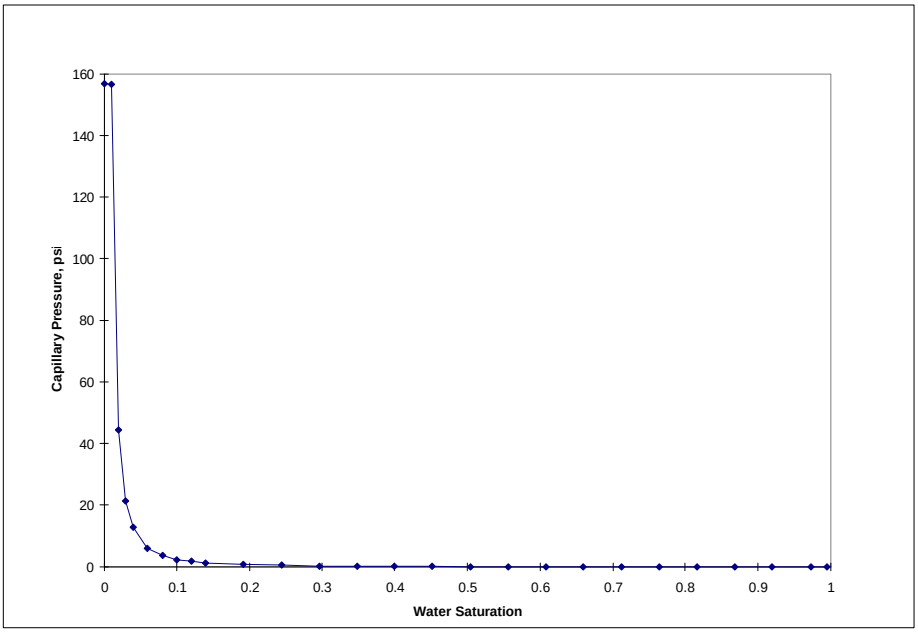

Figure 3.2: Brooks-Corey capillary pressure curve.

Figure 3.3 shows a comparison of the best results obtained from TOUGH2 and experimental measurement in terms of temperature. In the first 5 cm (from the heater), the simulated data match experimental measurements within $\pm 10^{o}$C. Except for the latest time curve, the simulated and experimental values match within $\pm 20^{o}$C along the rest of the length of the core. The maximum difference of 30^{o}C occurs at 19 cm (from the heater) at 476.6 hr.

The simulated steam saturation values agree with the simulated temperature profile (Figure 3.4). The saturation is equal to 1.0 when the fluid is superheated (i.e. in first 5 cm) at time=293.1 hr and time=476.6 hr. Except for time=46.9 hr, simulated and experimental steam saturation values vary within ±0.30 along the first 5 cm. The increasing trend in experimental steam saturation after 42 cm implies that air was present in the top layers of the core.

Pressure data are not included in this report because they were not use in the comparison between simulated and experimental results. Experimental pressure measurements were deemed problematic since many values were negative. This was probably due to water suction from the water vessel into the core when the steam front (closer to the heater) condensed upon meeting the cool water front (farther from the heater) within the core. After the steam had condensed, it left a void that needed to be filled.

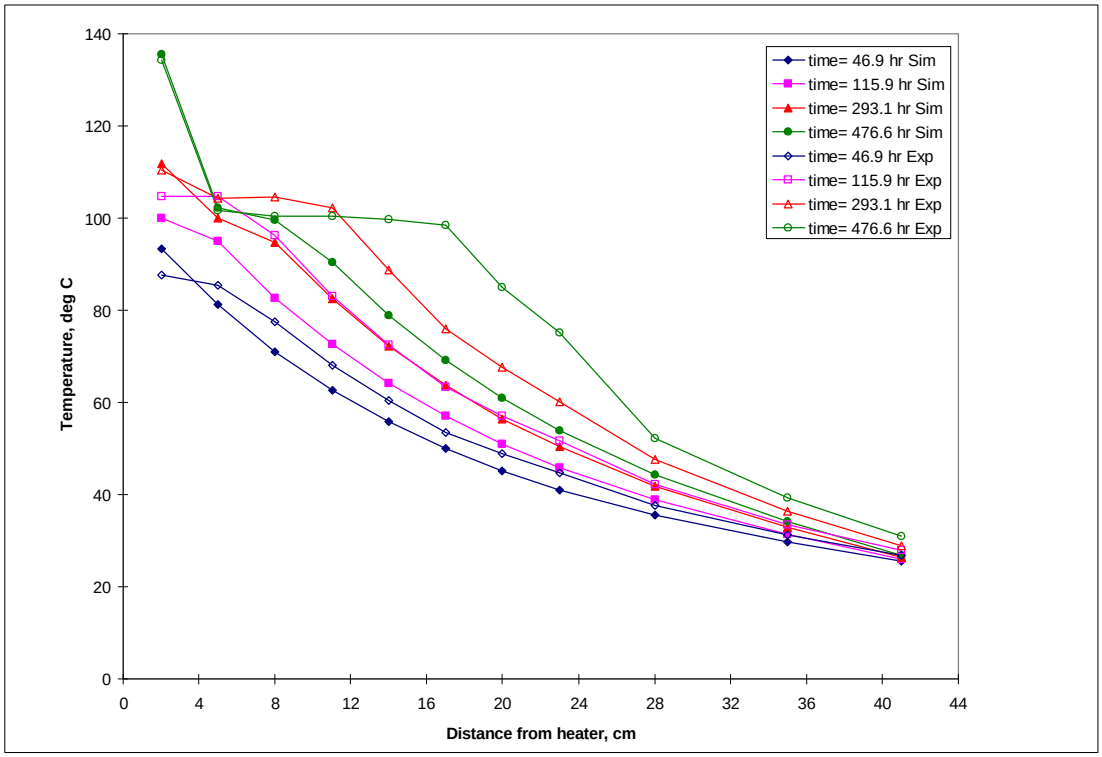

Figure 3.3: Temperature behavior along the length of the core.

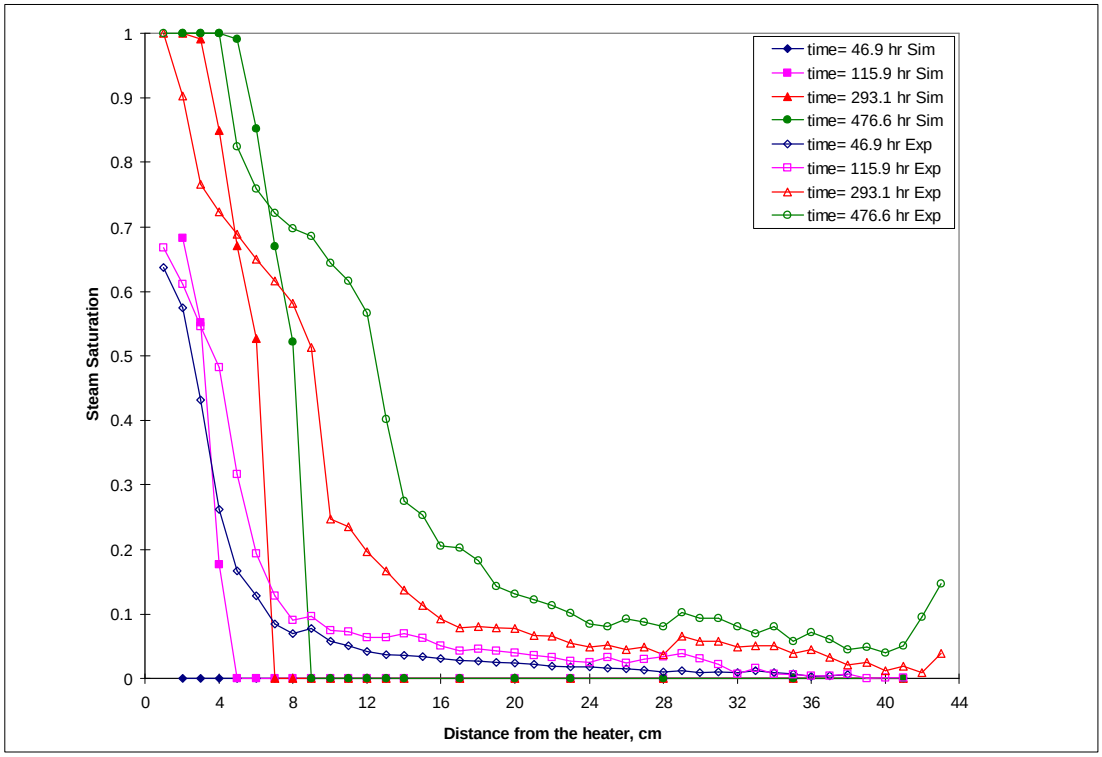

Figure 3.4: Steam saturation behavior along the length of the core.

3.5 FUTURE PLANS

Using the same TOUGH2 model, the more recent vertical experiments (described in Section 1) will be simulated to verify whether the Brooks-Corey relative permeability and capillary pressure functions can indeed be used for steam-water systems. Also, the Van Genucthen functions will be tried.

4. APPLICATION OF X-RAY CT SCANNING IN SATURATION AND POROSITY MEASUREMENT

This project is being conducted by Research Assistant Meiqing He, Dr. Cengiz Satik and Professor Roland Horne. The aim is to identify and to characterize fractures in geothermal rocks by using X-ray computer tomography (CT). The calculation of the porosity and the saturation process are closely related to fracture calibration. In earlier reports, we discussed the fundamental physics of the CT technique and proposed two ways of calculating porosity, here we propose a new method to reduce the noise in CT core images and to achieve subscale smoothing and interpolation by using the wavelet transform.

4.1 THEORETICAL BACKGROUND OF WAVELET TRANSFORM

Similar to the Fourier transform, the wavelet transform decomposes a time function on an orthogonal basis represented by a and t (variables which characterize the dilation and translation of the basic wavelet). The wavelet transform of a function $f(t) \in L^2(R)$ is defined by:

$$Wf(a,t) = \int_{-\infty}^{+\infty} f(t)\sqrt{a}y\ (a(t-t))dt \qquad (3.4)$$

where $y\ (t)$ is called a basic wavelet (mother wavelet). The translations and dilations form a family which is given by $\sqrt{a}y\ (a(t-t))$, which is an orthonormal basis.

Normally we are using the wavelet transform in a discretized form.

$$Wf(m,n) = 2^{\frac{m}{2}} \sum_k f(k)y\left(2^m k - n\right) \qquad (3.5)$$

In order to use this formula the signal has to in dyadic length, i.e., signal length N is equal to 2^J, where J is an integer.

In the wavelet multiresolution representation frame (Mallat, 1989), a signal is decomposed into approximations and details. The approximation at resolution $2^j\ (0 < j < J)$ is in space V_{2^j}, which is spanned by an orthogonal basis formed by the dilation and translations of $y\ (t)$. The difference between the approximations at resolution 2^j and 2^{j+1} is the detail signal at resolution 2^j, which belongs to the space O_{2^j}, the orthogonal complement of V_{2^j} in $V_{2^{j+1}}$. Space O_{2^j} is spanned by an orthogonal basis formed by the dilation and translation of a scaling function $j\ (t)$. Between $j\ (t)$ and $y\ (t)$, there is a pair of filters H and L, known as the quadrature mirror filter (QMF), to correlate them. There are many papers talking about how to construct the QMF and consequently obtain $j\ (t)$ and $y\ (t)$ with desired properties. In the pyramid algorithm, the approximations and details are obtained by cascade filtering using QMF. Figure 4.1 shows the scheme of decomposition. A_{2^j} and D_{2^j} denote the approximation and detail at resolution 2^j.

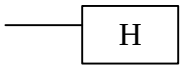

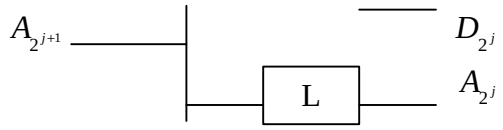

Figure 4.1: Scheme of decomposition.

For a two-dimensional signal, we assume the columns and rows are separable and the scaling function and wavelet function can also be constructed separately.

$$y^{1}(x,y) = y(x)j(y) \tag{4.3}$$

$$y^{2}(x,y) = j(x)y(y) \tag{4.4}$$

$$y^{3}(x,y) = y(x)y(y) \tag{4.5}$$

This construction corresponds to the filtering on column and row data sequentially.

The advantage of the wavelet transform over the conventional Fourier transform is that wavelets can form an unconditional base of many functional spaces. The wavelet transform gives us a way to analyze a signal at multiple resolutions.

Conventionally we filter noise in the frequency domain by reasonably assuming that the signal is banded and the noise is spread over the entire frequency domain. Usually we use a low-pass filter to cut out the high frequency noise. This procedure is based on the representation of the signal as a Fourier series. Theoretical proofs and experiments show that this representation is not very efficient. Often the Gibbs phenomenon (oscillation in rapid changing areas) is induced during such a process. By applying the wavelet transform, the signal is decomposed into its building blocks. In those wavelet coefficients, the signal coefficients rise above the noise level. Since the wavelet transform compresses the signal with finite energy l^2 into a smaller number of coefficient groups, the signal amplitude will stick up. Also the Gaussian white noise property is kept during orthogonal transformation, therefore the noise level remains the same. The amplitude of the noise level is proportional to $\sqrt{\log(n)}$, where n is the signal length (Donoho, 1993). We can take advantage of this property to filter the noisy wavelet coefficients while preserving the signal.

As an illustrative example, Figure 4.2 depicts the Gaussian noise effect in the wavelet coefficient domain. Field (a) shows the noisy block signal. (b) shows the true signal behind the noisy feature in (a). (c) and (d) display the wavelet coefficients obtained by transformation using a simple Haar wavelet. Correlating (c) and (d), we can tell that the signal coefficients do stand out of the noisy background. (e) displays the thresholded (filtered) wavelet coefficients. Comparing (e) with (d), the coefficients look similar to those of the original true signal.

In this project, we are going to apply the same wavelet transform procedure to CT image data to obtain a better representation of the true image.

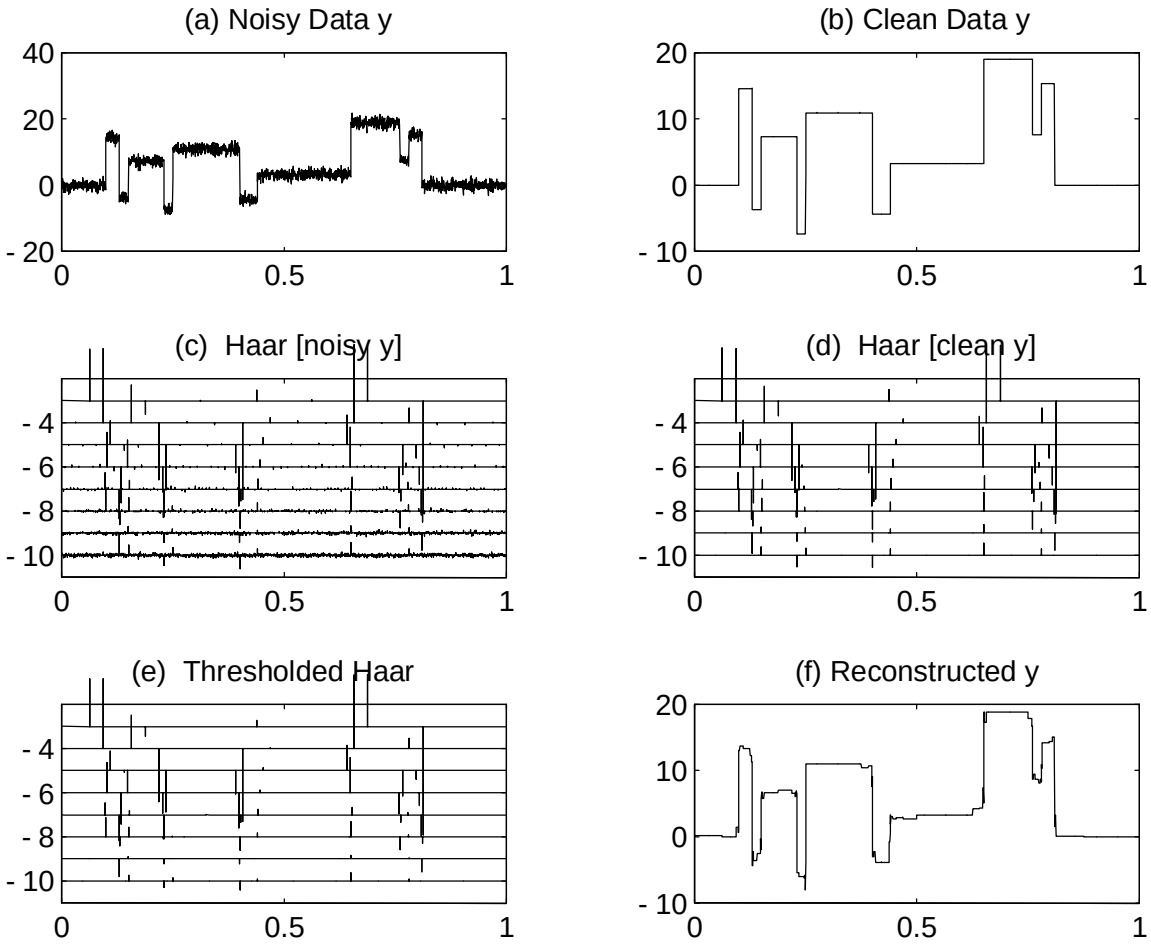

Figure 4.2: Comparison clean block signal and its noisy version in wavelet coefficients domain.

4.2 FUTURE WORK

We will study the properties of the noise in the X-ray detection process, which is known to be best represented as a Poisson distribution, and we will select appropriate wavelets and thresholds to reduce the noise in the wavelet domain of the CT image. We will also explore interpolation and refinement based on the use of the wavelet transform to obtain a higher resolution representation of the image.

5. PROPAGATION OF A BOILING FRONT IN A VERTICAL FRACTURE

This project is being conducted by Research Assistant Robert DuTeaux, Dr. Cengiz Satik and Prof. Roland Horne. The goal is to analyze the thermal front propagation associated with boiling in a vertical fracture. Improved understanding and modeling of heat transfer in a fracture will ultimately lead to better strategies for injection into fractured geothermal reservoirs.

5.1 INTRODUCTION

Previous reports have described the experimental setup and goals of this research. Over the summer the goals have been refined to more closely examine the two-phase zone that develops during boiling in a fracture, and the experimental apparatus and procedures have been improved. One experiment demonstrating boiling in a fracture was successfully conducted, but the results are not easily interpreted due to problems encountered with the apparatus, and with control of inlet temperature. These problems were the motivation for the redesign of both the experimental procedure and the experimental hardware.

5.1.1 Progress

The first experiment attempted last spring was unsuccessful due to high heat losses from the core of the assembly that allowed its surface (the fracture surface) to cool quickly. We therefore failed to initiate boiling in the fracture. Also, a leak in the outer evacuated region (designed for thermal insulation) pulled water out of the fracture annulus and into the vacuum annulus. These results suggested that modifications to the vacuum seal and changes in experimental procedure would improve the experimental results. Such changes were made this past quarter.

Despite these difficulties, the experimental apparatus successfully demonstrated two-phase flow and heat transport in the annulus between the two concentric glass tubes around the core of the assembly.

5.1.2 New experimental procedure and hardware

The heat losses that inhibited boiling were actually due to the thermal storage capacity of the apparatus. Because only the core of the apparatus was initially heated, the core holder assembly absorbed enough heat to cool the exterior surface of the core. This problem led to the idea of preheating the assembly with superheated steam before beginning the experiment.

Preheating the assembly was added to the procedure this past summer by incorporating a steam generator in parallel with the hot water generator. The intent of preheating was to allow the core and its holder, which form the two sides of the fracture, to begin in thermal equilibrium. However, in order to control the inlet steam temperature, a thermocouple was placed at the inlet and connected to a power control for the steam generator. Due to the failure of this feedback and control system the steam generator did not provide steam at a

consistently high temperature to preheat the apparatus. This was the main reason the experiments over the summer were not entirely successful.

The steam generator and valve allowed the apparatus to be preheated and then instantly switched to the injection of saturated liquid water. These components are shown in Figure 5.1.

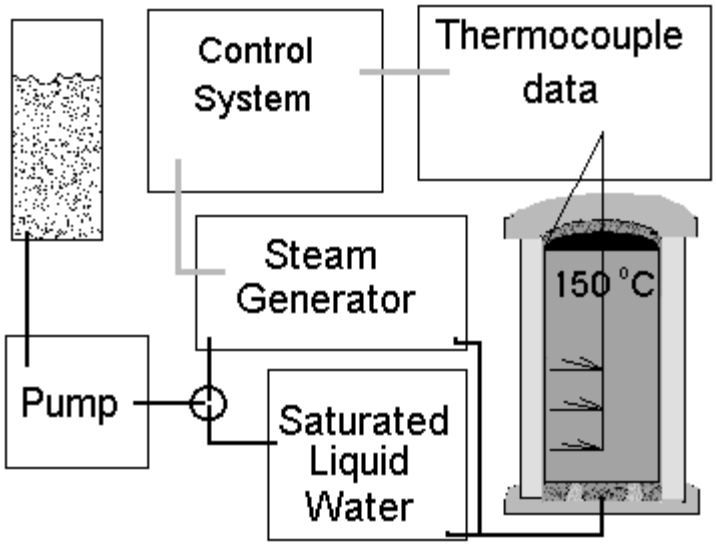

Figure 5.1: Experimental system design.

Thus, the new procedure began by using the steam generator to supply steam to preheat the apparatus. The core was preheated in an oven to a similar temperature in excess of 100°C and poured into the assembly. The experiment was then started by switching the valve at the pump exit from the steam generator to a supply of saturated liquid water. This saturated liquid then entered the apparatus and flowed up the fracture around the core. The excess temperature of the core caused the water to boil and thermocouples recorded the temperatures in the fracture, at the inner surface of the core, and radially inward toward the center of the core.

5.1.3 Vacuum seals

The original core assembly was sealed by compressing the ends of the glass tubes into silicone. This design had minor leaks from the fluid to the evacuated annulus during nearly every experiment. Due to thermal expansion during boiling, the magnitude of the leaks increased. At the beginning of the summer quarter it seemed that the best remedy for stopping leaks was to permanently seal the vacuum chamber with silicone without compression. However, this strategy was not successful.

After successfully demonstrating boiling in the annulus the experiment was disassembled and new O-ring seals were designed. The new O-rings were designed to seal both sides of the glass, rather than just the ends of the tubes, so that no direct leakage pathway exists. The new parts were machined but were not tested by the end of the summer quarter,

however, the new seals closely follow O-ring seal design and should not fail. These efforts should provide a much more robust experimental apparatus.

5.2 BOILING EXPERIMENT

Figure 5.2 is a sample of the data from the August boiling experiment. It shows the temperature history at a point 2.5 mm from the inner surface of the glass tube forming the fracture. The plot shows how the temperature changed quickly during the initial injection of fluid past the thermocouple position, which begins about 4 minutes after time zero. Because boiling caused enhanced convection, and because the latent heat of vaporization was absorbed from the core, the temperature changed very quickly early on. After the early transient are inflections in the temperature data that may reveal processes related to the location of two-phase flow, however, this measurement is not in the fluid itself, so this temperature plot is not a clear indication. Unfortunately, at the time this experiment was conducted the data acquisition system was monitoring but not recording the temperature data from the fracture annulus.

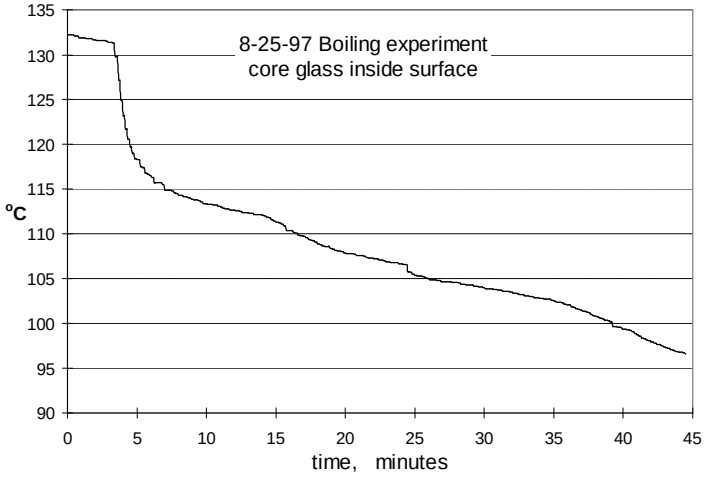

Figure 5.2: Glass temperature history at 2.5 mm radially inward from flowing fracture.

This temperature plot does illustrate the dramatic temperature effects of a thermal front caused by fluid flow passing a location in initially hot rock. We plan to repeat and analyze this thermal front and the extent of the two-phase zone.

After observing boiling in the apparatus, the size of the two-phase zone in the fracture became a topic for further investigation. Since boiling was nucleated at the ends of thermocouples and at rough grains within the otherwise smooth-walled fracture, the extent of the two-phase zone was not easily observed. The temperature measurements help to identify the isothermal zone at approximately atmospheric pressure, but its functional dependence on flow rate, orientation with respect to gravity, excess rock temperature and fracture geometry provide opportunities for further analysis.

5.3 THE NEXT STEPS

In the next quarter attempts to repeat the boiling experiment will be made and an effort to model the experiment numerically will contribute to a presentation of this work at the Stanford Geothermal Workshop early next year. Further investigation of the size of the two-phase zone in a fracture will also become more of a focus for further analysis if the functional dependencies can either be investigated experimentally or modeled.

Improvements in the data acquisition and control of the experiment are underway. Increasing the number of thermocouples being recorded is an immediate goal that will allow the fluid temperatures at discrete positions within the fracture to assist in identifying the extent of a two-phase zone. Measuring pressures has also been suggested.

6. MODELING OF GEOTHERMAL RESERVOIRS CONSTRAINED TO INJECTION RETURN DATA

This project is being conducted by Research Assistant Ma. Michelle Sullera and Prof. Roland Horne. It aims to deduce injection return mechanism(s) and flow paths from correlations between producer chloride concentration and injection operating parameters (flow rate and injection chloride).

6.1 BACKGROUND

Previously, production and injection data from both Palinpinon-I geothermal field in the Philippines and Dixie Valley field were analyzed using the following models:

CORRELATION 1

$$Cl_p = a_0 + a_1 Q_{I1} + a_2 Q_{I2} + a_3 Q_{I3} + \ldots \quad + a_n Q_{In} \tag{6.1}$$

CORRELATION 2

$$Cl_p = a_0 + a_1 Q_{I1} + a_2 Q_{I2} + a_3 Q_{I3} + \ldots \quad + a_n Q_{In} + bt \tag{6.2}$$

where Cl_p = chloride concentration in production well, P

Q_{In} = mass flow rate to injection well, In

a_n = linear coefficient of well In

a_0 = a constant associated with local chloride concentration

t = time

It was shown that Correlation 2 fits the data better than Correlation 1; however, Correlation 2 was also shown to have a poor 'predicting capacity.'

6.2 CONTINUING WORK

This project will now continue along a different path, using numerical simulation to replace the heuristic flow models. Results of the linear correlation work will be incorporated in a multicomponent (water + chloride) numerical model of the Dixie Valley reservoir. The degree of connectivity between producers and injectors deduced from Correlation 2 will be modeled by varying the permeability of blocks between these wells. What gives rise to the linear relationship between producer chloride concentration and injection rates? Are these linear correlations equivalent representations of high permeability channels? How do we model the negative coefficients previously calculated? These are questions we will address in the ongoing numerical modeling work.

7. REFERENCES

Donoho, D.L., "Nonlinear Wavelet Methods for Recovery of Signals, Densities, and Spectra from Indirect and Noisy Data", *Proceedings of Symposia in Applied Mathematics, Vol. 00, 1993.*

Mallat, S.G., "A Theory for Multiresolution Signal Decomposition: The Wavelet Representation", *IEEE Transaction on Pattern and Machine Intelligence, Vol.11, No. 7, July 1989.*

Satik, C., 1994, "Studies in Vapor-Liquid Flow in Porous Media", *Ph.D. Thesis*, University of Southern California, Los Angeles, CA.

Satik, C., 1997, "Experiments of Boiling in Porous Media", Proc. of 22nd Stanford Workshop on Geothermal Reservoir Engineering, Stanford, CA.

Satik, C. and Yortsos, Y.C., 1996, "A Pore Network Study of Bubble Growth in Porous Media Driven by Heat Transfer", *J. Heat Transfer,* **118.**